Radiocarbon, Vol 61, Nr 3, 2019, p 661–680 DOI:10.1017/RDC.2019.27

$\Delta^{14}C$ AND $\delta^{13}C$ IN ANNUAL TREE-RING SAMPLES FROM *SEQUOIADENDRON GIGANTEUM*, AD 998–1510: SOLAR CYCLES AND CLIMATE

C J Eastoe[1]* · C S Tucek[1] · R Touchan[2]

[1]Department of Geosciences, University of Arizona, Tucson, AZ 85721, USA (retired)
[2]Laboratory of Tree-Ring Research, University of Arizona, Tucson, AZ 85721, USA

ABSTRACT. Time series of annual $\Delta^{14}C$ and $\delta^{13}C$ in tree rings of *Sequoiadendron giganteum*, AD 998–1510, are similar in form. The $\Delta^{14}C$ series completes, with data of Stuiver and Braziunas (1993), a 957-yr time-series. Discrete Fourier transformation of detrended $\Delta^{14}C$ reveals periods of 126, 91, 56, 17.6, 13.6, 10.4, and 7.1 yr. Non-random differences exist between decadal averages of the *Sequoiadendron* $\Delta^{14}C$ data and data of Stuiver and Becker (1993). Periods of 7–17 yr may correspond to Schwabe or related climatic cycles; these have 10–17-yr periods and amplitudes < 6‰ (AD 1100–1250), and periods near 7 yr with amplitudes up to 10‰ (AD 1380–1420). Abrupt increases in $\Delta^{14}C$ are mainly less than 5‰, and do not constitute convincing evidence of increased ^{14}C production from supernovae or solar proton events. The $\delta^{13}C$ time-series is likely to reflect climate change, and for centennial periodicity lags behind $\Delta^{14}C$ by 20–40 yr (centennial time-scale) and 25–50 yr (millennial). Phase-shifts between solar luminosity and surface $\Delta^{14}C$ are 125–175 yr and 20 yr for millennial and centennial cycles, respectively. The study suggests that strongest climate effects may therefore follow peak luminosity by 125–175 yr for millennial cycles and 20–40 yr for centennial cycles.

KEYWORDS: carbon-13, carbon-14, climate change, solar cycles, tree rings.

INTRODUCTION

Cellulose in tree rings preserves an archival record reflecting the carbon isotope content of the atmosphere. In long-lived species with broad annual rings, it is possible to extract sufficient carbon for high-precision liquid scintillation measurement of ^{14}C content in single rings, in addition to routine measurement of $\delta^{13}C$. Examples include records for Douglas fir (*Pseudotsuga menziesii*) sampled in the Pacific Northwest, USA, for tree rings spanning the interval AD 1500–1953 (Stuiver and Braziunas 1993; data republished with corrections by Stuiver et al. 1998), for the giant sequoia (*Sequoiadendron giganteum*) of California for the years AD 1065–1150 (Damon et al. 1998) and AD 1688–1710 (Damon et al. 1999). More recently, high-precision data measured by accelerator mass spectrometry (AMS) have been presented for single tree rings from Japanese cedar (*Cryptomeria japonica*) for AD 600–1021 (Miyake et al. 2012, 2013a, 2013b) and AD 1415–1629 (Miyahara et al. 2004, 2006, 2007), and from European oak for AD 1010–1110 (Güttler et al. 2013). In other cases, where material was insufficient for annual measurement or where annual samples were not feasible over a long time interval, ^{14}C content has been measured in decadal and bidecadal tree-ring samples (e.g. Stuiver and Becker 1993, data republished with corrections by Pearson et al. 1986; Stuiver et al. 1998; Pearson and Qua 1993, data republished with corrections by and McCormac et al. 1998). Reimer et al. (2004) discussed the reasons for corrections to early datasets.

Such datasets have been applied (1) to the calibration of the radiocarbon time scale (Stuiver and Becker 1993); (2) in conjunction with measurements of ^{10}Be in ice cores (Oeschger and Beer 1990; Raisbeck et al. 1990; Bard et al. 1997; Beer et al. 2012), to the identification and explanation of abrupt, cyclic and secular changes in atmospheric ^{14}C content (Damon and Sonnett 1991, and references therein); and (3) to examining connections between changes in the solar magnetic field and modulation of ^{14}C production at multi-decadal time scale (Miyahara et al. 2008). Changes in the ^{14}C content of the atmosphere at Earth's surface

*Corresponding author. Email: eastoe@email.arizona.edu.

reflect changes in the rate of generation of ^{14}C in the upper atmosphere, and also in the distribution of CO_2 among near-surface reservoirs (Damon and Sonnett 1991; Stuiver and Braziunas 1993).

Datasets with annual resolution have been searched for evidence of short-term changes in the rate of generation of ^{14}C, such as might result from the 11-yr Schwabe cycle of solar activity (Stuiver and Braziunas 1993; Miyahara et al. 2004, 2006, 2007, 2009), from supernovae (SN) in the galactic neighborhood (Damon et al. 1995a, 1995b), or from solar proton events (SPEs) generated by giant solar flares (Miyake et al. 2012, 2013b). Recent interest has focused on an abrupt increase of 14‰ in $\Delta^{14}C$ at AD 774–775 (Miyake et al. 2012) and another of 9‰ at AD 994–995 (Miyake et al. 2013b). The AD 774–775 event was global in effect (Jull et al. 2014). Explanatory hypotheses include an SPE, a gamma-ray burst from beyond the solar system, and collision of a comet with the Sun or the Earth; of these, an SPE appears most plausible (Jull et al. 2014, and references therein).

The contribution of solar luminosity cycles to climate change is receiving close scrutiny in the context of present climate change (Masson-Delmotte et al. 2013; Myhre et al. 2013). In this context, long-term trends in $\delta^{13}C$ are of interest because $\delta^{13}C$ records in tree rings are used in climatic reconstructions (Leavitt 2010 and references therein). None of the tree-ring archive studies cited above included a $\delta^{13}C$ dataset with the published ^{14}C record, notwithstanding the necessity of measuring $\delta^{13}C$ in order to correct the ^{14}C measurements (Stuiver and Polach 1977). Stuiver and Braziunas (1987) considered a 2000-yr dataset of $\delta^{13}C$ measurements in tree rings at decadal resolution, without reference to ^{14}C measurements. Shorter-term studies of $\delta^{13}C$ in sub-annual portions of tree rings, preferably samples from multiple individuals in a study area, are a staple of dendrochronology (Leavitt 2010).

In this article, we present the results of a study initiated by the late Professor Paul Damon in the 1980s. The study has produced high-precision measurements of ^{14}C and routine measurements of $\delta^{13}C$ in annual tree-ring samples from a giant sequoia for the years AD 998–1510. Objectives of the study included (1) assembly and time-series spectral analysis of the high-precision dataset; (2) analysis of the differences between the new dataset and a set of decadal measurements (Stuiver and Becker 1993) spanning the same time interval; (3) interpretation of short-term fluctuations in the ^{14}C data in the context of identifying decadal and shorter events such as supernovae, giant solar flares and the Schwabe cycle; and (4) examination of the relationship of $\delta^{13}C$ and $\Delta^{14}C$ records and its implications for climate change.

BACKGROUND

Study Area

Material for the study was obtained from a fallen sequoia in the Big Stump Grove (36.75°N, 118.97°W, altitude 1850 m above sea level, masl) in the southern Sierra Nevada Mountains, California, USA. Prior dendrochronological studies in the area include determinations of temperature over the past 2000 yr from *Pinus balfouriana* collected at the tree-line at Cirque Peak, about 70 km southeast of Big Stump grove (Scuderi 1993), and determinations of temperature and precipitation records over the past 1000 yr from *Pinus balfouriana* and *Juniperis occidentalis* at tree-line sites, 3300–3400 masl, between 40 and 60 km southeast of Big Stump Grove (Graumlich 1993). The derived temperature records differ greatly. Hughes et al. (1996) presented a multi-millennial tree-ring chronology for

https://doi.org/10.1017/RDC.2019.27 Published online by Cambridge University Press

sequoias from multiple locations, and noted the consistency of low-growth years between sites. Hughes and Brown (1992) interpreted low-growth years in terms of drought frequency in central California since 101 BC. Swetnam and Baisan (2003) evaluated the record of fire preserved in tree rings from the Big Stump Grove and neighboring sequoia groves, finding the highest frequency of widespread fire in the interval AD 1000–1200. Craig (1954) presented a set of $\delta^{13}C$ values for the central wood of tree rings from a sequoia from Springville, California, representing the period 1072 BC to AD 1649. The samples are spaced at intervals of 50 yr or more since AD 1000.

Previous Work on the Current Dataset

Several progress reports have arisen from parts of the dataset, which was collected between 1992 and 2006. Spectral analysis of the data for the Late Medieval Solar Maximum was presented by Damon et al. (1998) and Damon and Peristykh (2000). A pattern of ^{14}C data thought to correspond to the SN of AD 1006 was discussed by Damon et al. (1995a, 1995b) and Damon and Peristykh (2000). Kalin et al. (1995) compared annual ^{14}C data for the 11th and 12th centuries with decadal data from other laboratories.

Contemporaneous Datasets

Stuiver and Becker (1993) presented high-precision decadal ^{14}C data for tree rings spanning the interval 6000 BC to AD 1950. These and decadal or bidecadal data of Pearson and Qua (1993) overlap the annual data presented here, and form the basis of calibration of the last 8000 yr of the radiocarbon time scale. The AMS data of Miyake et al. (2013a) and Miyahara et al. (2004) overlap the present dataset from AD 998–1021 and AD 1415–1510.

Cosmogenic Isotopes, Solar Activity, and Climate

It has long been recognized (Damon and Sonnett 1991 and references therein) that records of cosmogenic isotopes archived at Earth's surface reflect interaction of three groups of factors: (1) long-term changes in the dipole moment of Earth's magnetic field, (2) changes in the fluxes of cosmic radiation and charged particles of solar origin, modulated by interaction of the solar wind with Earth's magnetic field, and (3) changes in the geochemical cycle of each cosmogenic isotope. The following summary of the interplay of these factors for the isotopes ^{10}Be and ^{14}C is based on Beer et al. (2012, Chapter 17).

After low-pass filtering, time series of ^{10}Be and ^{14}C show similar form at the time scale of the Holocene (Bard et al. 1997; Figure 17.3.2–1 of Beer et al. 2012), and since AD 1600 (Figure 17.2.1–1 of Beer et al. 2012). In the latter case, the time series can be compared with sunspot numbers, a direct measure of solar activity. The production rate of each isotope is inversely related to sunspot number. High sunspot number corresponds to high solar luminosity, the luminosity being the net sum of radiation increases due to bright solar faculae and decreases due to dark sunspots. Higher solar activity also corresponds to high intensity of the solar wind, leading to attenuation of the flux of galactic cosmic rays into Earth's upper atmosphere. High solar activity therefore leads to two interdependent effects on Earth: decreased abundance of cosmogenic isotopes, and increased total solar irradiance (TSI). The ^{10}Be time series, archived in stratified polar ice, has the advantages of a close relationship with solar activity and little attenuation arising from the geochemical cycle of Be, but the disadvantage of imprecise chronology. The ^{14}C time series, archived in tree rings, has the advantage of precise chronology. However, the signal ^{14}C originating from

https://doi.org/10.1017/RDC.2019.27 Published online by Cambridge University Press

cosmogenic production is attenuated and delayed relative to the ^{10}Be signal as a result of cycling of carbon among surface reservoirs, particularly transfers to and from the deep oceans. Attenuation and phase-shift are functions of the period of the cosmogenic production signal, and have been estimated from 5-box and 3-box models of the surface carbon cycle (Houtermans et al. 1973; Damon and Peristykh 2004; Usoskin and Kromer 2005; Beer et al. 2012, Figure 13.5.3.2–2). The ^{14}C time series as archived at Earth's surface may be complicated by any modification of climate (leading to changes in the carbon cycle) arising from changing TSI (Damon and Sonnett 1991). Whether changes in solar activity affect climate significantly will be addressed in the Discussion.

METHODS

Wood samples were collected and subjected to dendrochronological analysis by researchers at the Laboratory of Tree-Ring Research at the University of Arizona. Individual tree-ring samples, ideally 40–60 g, were separated as chiseled flakes at the Laboratory of Tree-Ring Research, University of Arizona, under the supervision of Dr. Ramzi Touchan. Each sample represents much of the circumference of a whole tree-ring. The flakes were ground in a Wiley® mill. Cellulose was prepared from the wood in two stages: first, leaching of components soluble in a toluene-ethanol mixture in a Soxhlet® distillation apparatus; second, bleaching of remaining non-cellulose components in an aqueous solution of sodium chlorite. Ideally, the resulting fraction of cellulose amounted to 20–25 g. Details of the method are given in Kalin et al. (1995).

In the intervals AD 1065–1070, 1073–1074, 1126–1135, 1143–1144, 1189–1190, and 1256–1265, the tree rings were narrow, requiring the combination of two rings to make a sufficient sample. Samples that were too small for liquid scintillation counting (AD 998–1024 and a few samples for which most of the cellulose was lost in laboratory mishaps), were measured on 3 to 5 graphite targets at the NSF-Arizona AMS facility. For the years AD 1096, 1136, 1366, and 1372, all sample material was lost and no measurements could be made.

Samples of sufficient size, ideally 7 g of benzene, were prepared for liquid scintillation counting (LSC) following a method designed to minimize impurities in the benzene product (Witkin 1992). Details of the method and characteristics of counting vials are provided as supplementary material, including Table S1.

Data are presented as Δ^{14}C (Stuiver and Polach 1977). An error (1σ) of ± 2‰ or better was routine for LSC over most of the study. Using standard statistical formulae, errors were calculated from machine error of a given measurement in combination with long-term statistics for standard and background measurements. In the interval AD 1065–1141, several samples have errors in the range ± 2.0 to 2.5‰. In the case of samples measured by AMS, results are presented as the mean, weighted for variance, of measurements on three or more targets, and the standard error of the mean. Errors of AMS data ranged from ± 2.5 to 4.7‰, the larger errors being limited to the interval AD 998–1024. Results were standardized relative to international standards Oxalic Acid I (LSC) and Oxalic Acids I and II (AMS).

Values of δ^{13}C were determined on a portion of the CO_2 prepared for ^{14}C measurement and were used to correct the ^{14}C data for variable isotope fractionation, for instance in photosynthetic uptake of CO_2 as a result of climatic stress. Prior to 1995, the δ^{13}C measurements were made using a modified VG® 602C dual-inlet gas source mass

https://doi.org/10.1017/RDC.2019.27 Published online by Cambridge University Press

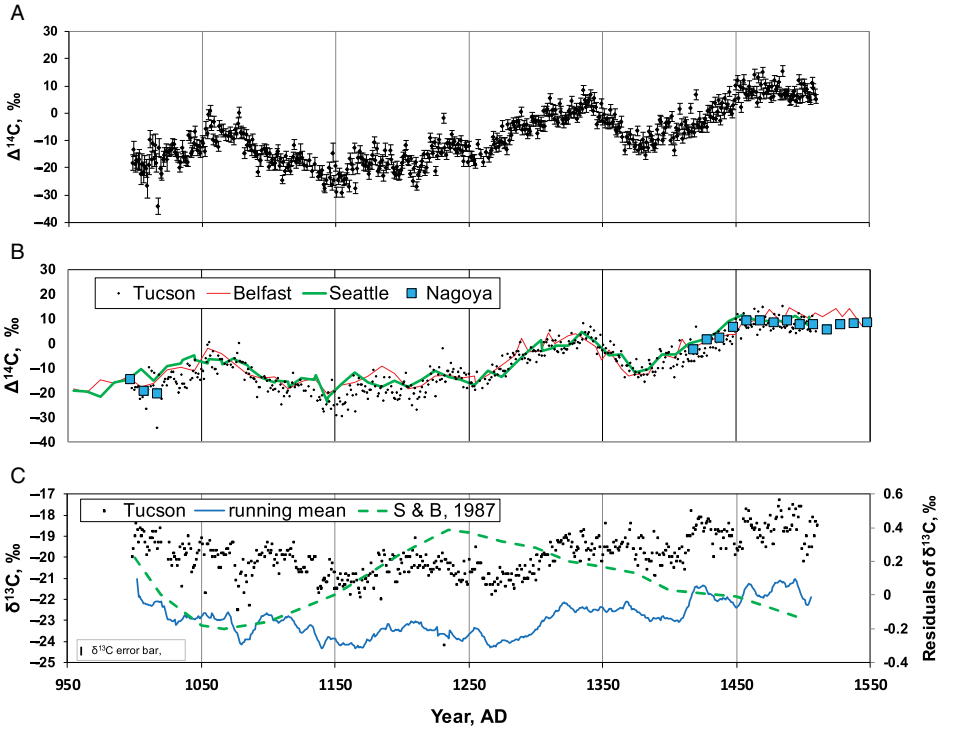

Figure 1 A. The Tucson $\Delta^{14}C$ time series, with error bars (1σ). B. Comparison of the Tucson $\Delta^{14}C$ time series (points) with the decadal Seattle and the decadal/bidecadal Belfast $\Delta^{14}C$ time series (both represented as lines). C. The Tucson $\delta^{13}C$ time series, with a 10-yr running mean displaced downward by 5‰. Also shown is the time series of average residuals of $\delta^{13}C$ in a variety of North American tree species (Stuiver and Braziunas 1987).

spectrometer, with an analytical precision (1σ) of 0.15‰. Since 1995, measurements were made on a Finnigan® Delta-S dual-inlet gas source mass spectrometer, with an analytical precision (1σ) of 0.10‰. Results were standardized relative to standards NBS 22 and USGS 24.

RESULTS AND COMPARISONS WITH OTHER DATASETS

The data (supplementary Table S2) are presented as paired measurements of $\Delta^{14}C$ and $\delta^{13}C$, and are depicted as a time-series of annual $\Delta^{14}C$ and $\delta^{13}C$ in Figure 1, where the data (referred to as the Tucson dataset below) are compared with (1) contemporaneous decadal data for Douglas fir samples, collected in the Pacific Northwest and measured at the University of Washington (the Seattle dataset: Stuiver and Becker 1993; Stuiver et al. 1998), and (2) contemporaneous bidecadal data for Irish oak samples measured at Queen's University, Northern Ireland (the Belfast dataset: Pearson et al. 1986; McCormac et al. 1998). In Figure 2, the Tucson and Seattle annual datasets are combined with annual data (and some decadal data, or data averaged over decadal intervals, for clarity) from the Nagoya laboratory (Miyahara et al. 2004; Miyake et al. 2012, 2013a, 2013b) to provide a record from AD 600 to 1953. Systematic differences exist between LSC $\Delta^{14}C$ measurements from contemporaneous sets of tree rings from different continents, regardless of the laboratory that made the measurements (McCormac et al. 1995). An early evaluation based on non-corrected data from Seattle and Belfast and a partial Tucson dataset (Kalin et al. 1995)

https://doi.org/10.1017/RDC.2019.27 Published online by Cambridge University Press

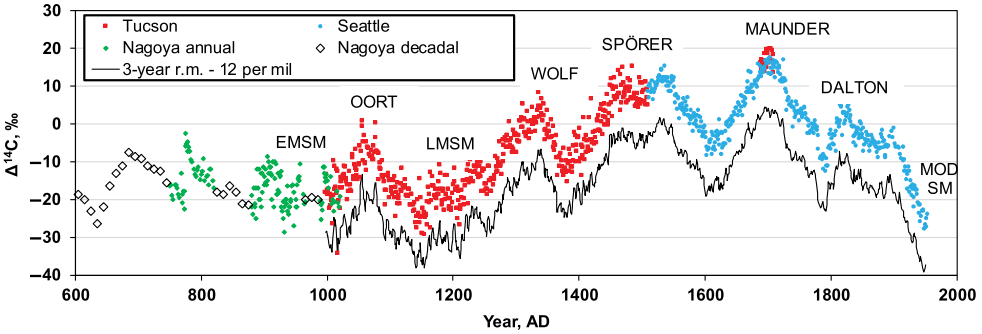

Figure 2 Annual and decadal $\Delta^{14}C$ time series for tree rings since AD 600 (Tucson laboratory: this study; Seattle laboratory: Stuiver et al. 1998; Nagoya laboratory; some data expressed as decadal means: Miyahara et al. 2004; Miyake et al. 2012, 2013a, 2013b), with a 3-yr running mean (displaced downwards by 12‰) for AD 998–1954. Named Grand Solar Minima and Maxima are shown. E(L)MSM = Early (Late) Medieval Solar Maximum, MOD SM = Modern Solar Maximum.

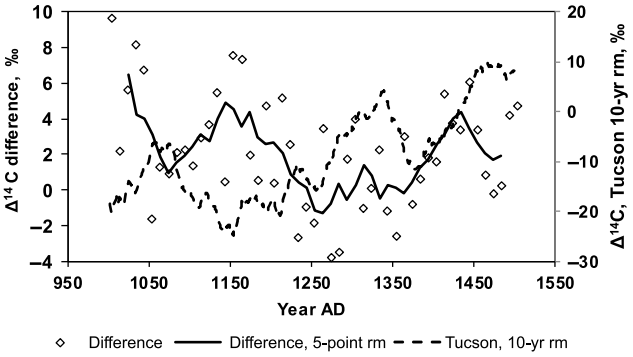

Figure 3 Time series of differences between the Seattle decadal dataset of $\Delta^{14}C$ and the Tucson dataset expressed as decadal averages (Seattle minus Tucson), compared with a 10-yr running mean (rm) of the Tucson $\Delta^{14}C$ time series.

concluded that there was a satisfactory agreement between the Tucson and Seattle data, but noted a systematic offset between data from Tucson and Belfast. Damon et al. (1998) calculated a mean difference (non-corrected Seattle data minus Tucson data) of 1.0 ± 2.1‰ for decadal averages over the period AD 1065–1145, and concluded that the difference was well within error. Applying the same approach to the entire Tucson dataset and the corrected Seattle data, the average difference is 2.2 ± 3.2‰. The three datasets (Figure 1B) match in general, but show systematic differences over certain periods of several decades (Figure 3, for Seattle and Tucson data).

For the Seattle measurements, each of which represents a single, high-precision decadal measurement, the typical standard deviation (1σ) is 2.5‰. For the decadal means calculated from the Tucson dataset, values of σ are calculated as standard errors of each decadal mean of $\Delta^{14}C$ (supplementary Table S3). The typical value of σ for the difference

https://doi.org/10.1017/RDC.2019.27 Published online by Cambridge University Press

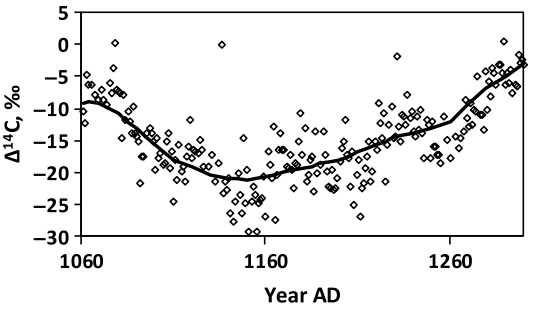

Figure 4 $\Delta^{14}C$ data for the Late Medieval Solar Maximum: Tucson dataset, annual data (points) with a smoothing spline (line) with gain 0.95 and a period of 200 yr.

(Seattle-Tucson) is between 2.6 and 2.9 ‰ (Table S3). The range of the decadal differences in Figure 3 is 14‰.

If the differences arose from measurement error only, their scatter as a function of time would be random. Such is not the case; whether the differences are depicted as individual points or moving averages, there appears to be a cyclic change in the magnitude of the differences, and the change is inversely related to the decadal means for the Tucson data (Figure 3). The cyclic variation of difference between the two datasets appears to be real, in that the extremes of difference are statistically different. Comparing the extended Tucson dataset with the Seattle decadal data suggests that systematic, cyclic differences, possibly climatic in origin, exist between the Pacific Northwest and the Sierra Nevada. The Tucson $\delta^{13}C$ time-series (Figure 1C) shows a long-term change broadly matching that of the $\Delta^{14}C$ data, and shorter cyclic variations.

SPECTRAL ANALYSIS

The data in the vicinity of the Late Medieval Solar Maximum have been detrended by (1) calculation of a smoothing spline for T = 200 yr (Figure 4) which has the effect of removing cyclic variations of T/2 or less, and (2) subtraction of the spline from the dataset, leaving the short-period cycles without long-term trends (Figure 5). A period near 55 yr is clearly seen, along with cycles with T near 10 yr. This shorter cycle has intervals of low amplitude near AD 1130 and 1240, suggesting amplitude modulation with T near 110 yr.

Discrete Fourier Transformation (DFT) of the detrended data (modified by subtraction of the smoothing spline for T= 200 yr) shows strongest peaks at 126, 91, 56, 17.6, 13.6, 10.4, and 7.1 yr (Figure 6). Amplitudes < 0.5 units appear to be noise; only peaks of greater amplitude are labeled with the corresponding period in years. Periods less than 5 yr are probably spurious.

The distribution of short-T variations in time can be seen in the spectrogram (Figure 7) constructed using a 77-yr moving window. Periods near 7 yr are most in evidence during the interval AD 1320–1450. Periods of 10–17 yr are most prominent during the interval AD 1000–1120. A 56-yr period persists between AD 1000 and 1200 and from 1350 to 1400, but is weak or absent at other times.

https://doi.org/10.1017/RDC.2019.27 Published online by Cambridge University Press

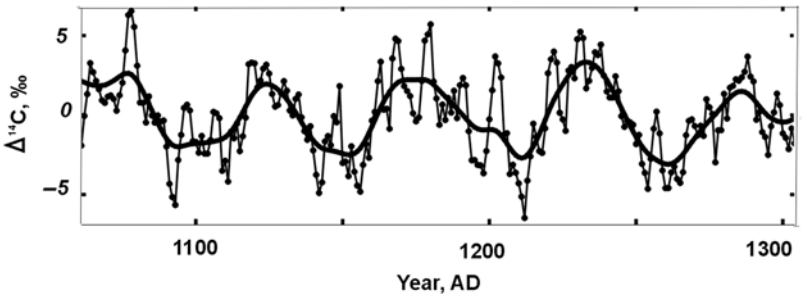

Figure 5 $\Delta^{14}C$ data for the Late Medieval Solar Maximum: Tucson dataset, annual data, detrended by subtraction of the smoothing spline in Figure 4.

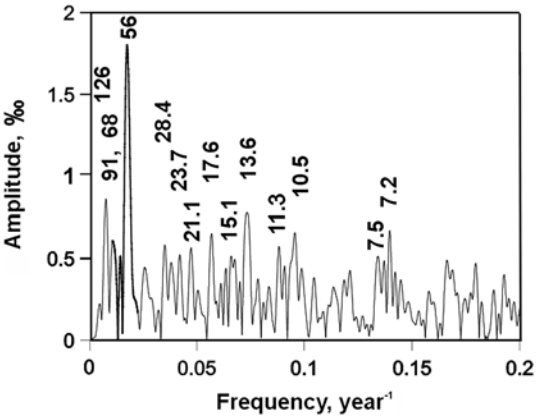

Figure 6 Discrete Fourier Transform power spectrum of the detrended Tucson $\Delta^{14}C$ dataset. Larger peaks are labeled with the corresponding period in years.

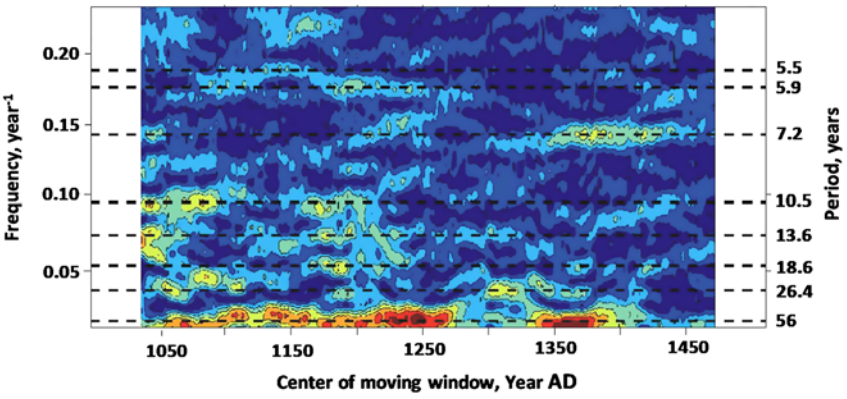

Figure 7 Spectrogram of Tucson $\Delta^{14}C$ data (frequency vs. time plot showing contours of Discrete Fourier Transform spectral amplitude for a 77-yr time window). Yellow and enclosed colors indicate high amplitudes. Horizontal dashed lines mark prominent periods.

https://doi.org/10.1017/RDC.2019.27 Published online by Cambridge University Press

COMPARISON WITH ANNUAL DATA, AD 1510–1954

Considering cyclicities between the 88-yr Gleissberg cycle and 5 yr, Stuiver and Braziunas (1993) noted periods of 56, 26, 17, 13.2, 10.4, 6.4, 5.7, and 5.1 yr in the Seattle annual dataset for AD 1510–1954. This set of periods compares closely with the Tucson power spectrum for T > 5 yr. As discussed above, the Seattle and Tucson laboratories produce data that appear to be comparable in accuracy and precision, but the raw Tucson data in Figure 2 appear to show greater scatter than the Seattle data. Whether this arises from the raw material or from experimental technique is unclear. If there were greater scatter due to error in the Tucson data, however, the error should be random and would be attenuated by smoothing. Figure 2 shows that smoothing in fact results in the detection of non-random cyclic variations in both datasets. The cycles are the 7–17-yr periods described above, and their amplitude, particularly between AD 1000 and 1300, is larger than that of corresponding periods in the Seattle data. Outlying results (supplementary Table S2), present in the Tucson dataset to a greater degree than in the Seattle dataset, include five large jumps in $\Delta^{14}C$ at AD 1017 (negative jump, AMS measurement), AD 1160 (negative, LSC), AD 1165 (negative, LSC), AD 1231 (positive, LSC), and AD 1420 (positive, LSC). Laboratory contamination might be expected to shift $\delta^{13}C$ either positively (atmospheric contamination) or negatively (contamination from pre-treatment chemicals); however, only the outlier at AD 1231 has a $\delta^{13}C$ value markedly different from neighboring data. Large jumps in $\Delta^{14}C$ are present in comparable datasets (Miyahara et al. 2004, 2009; Miyake et al. 2012). Whether the outliers in the Tucson dataset result from experimental shortcomings or from the nature of the raw samples remains unclear. The data are presented here without censoring.

SHORT-TERM EVENTS

Annual time-series data are of use in identifying decadal cyclic phenomena such as the Schwabe and Hale cycles of solar activity, and non-cyclic phenomena of similar time-scale, for example the generation of ^{14}C pulses by SPEs from large solar flares. The cyclic phenomena are expected to approximate sinusoids, while the non-cyclic events may appear as abrupt single-year changes followed by slower reversal of the initial change, approximating a single cycle of a square wave. The latter are termed stepwise changes below.

Sinusoid-Like Cycles

Cycles of T = 10–17 yr (Figure 7) and amplitudes of 3–6‰ (Figure 6) are most visible in the Tucson dataset in the Late Medieval Solar Maximum. Such amplitudes are comparable to the 4‰ expected to result at Earth's surface from atmospheric low-pass filtering of variations due to the Schwabe cycle (Damon and Sonnett 1991). For sinusoidal signals of T near 10 yr, the attenuation factor is near 100 and the phase shift is about 2 yr (Damon and Peristykh 2004; Usoskin and Kromer 2005). Between AD 1350 and 1450, T near 7 yr predominates (Figure 7) and amplitudes of 10‰ or more may be present, notwithstanding the larger expected attenuation of a 7-yr period relative to a 10-yr period (Damon and Peristykh 2004; Usoskin and Kromer 2005).

For comparable periods, amplitudes less than 5‰ are present in the Seattle and Nagoya datasets (Stuiver and Braziunas 1993; Miyahara et al. 2004, 2006, 2007, 2009), but periodicity is less regular than at the Late Medieval Solar Maximum. Güttler et al. (2013) reported cycles with T = 12 yr and amplitudes near 2‰ in the interval AD 1010–1110.

https://doi.org/10.1017/RDC.2019.27 Published online by Cambridge University Press

Note that Kocharov (1992) reported amplitudes of 10‰ or greater for cycles of approximately 10-yr period in a single-yr $\Delta^{14}C$ time series for AD 1600 onwards; such large amplitudes are not seen in the contemporaneous Seattle dataset. Stuiver and Braziunas (1993) proposed a combination of modulation of $\Delta^{14}C$ production by the solar wind and modification of the carbon cycle by North Atlantic thermohaline circulation as an explanation for observed spectral power corresponding to the Schwabe cycle.

Modulation of $\Delta^{14}C$ by the solar wind appears to be a sufficient explanation of the amplitudes and periods of the cycles depicted in Figure 6. However, it is surprising, considering the routine 1σ analytical precision near 2‰, that the observed amplitudes of 3–6‰ are preserved in the Tucson and other datasets. Random errors might be expected to disrupt the sequential increases and decreases in $\Delta^{14}C$ (Figure 6). The larger amplitudes and shorter periods in the interval AD 1380–1420 may reflect a climatic influence, as yet unexplained, on the surface carbon cycle. At present, it remains unclear whether the short-period variations reported here are indeed related to the Schwabe cycle.

Stepwise Events

The AD 1006 SN, observed optically, may have produced the stepwise increase in $\Delta^{14}C$ of about 8.5‰ at AD 1010–1011 in our time-series of $\Delta^{14}C$ (Damon et al. 1995a, 1995b), followed by gradual decay over a decade. The delay between the arrival of visible light and gamma radiation may have resulted from a delay in the arrival of gamma rays relative to visible light (Damon et al. 1995a, 1995b), but may be partly explained by phase shift due to low-pass filtering. If this pulse of radiation is considered as a square wave of period 12 yr, its principal sinusoidal component also has a period of 12 yr, with a phase shift of about 2 yr and an attenuation factor comparable to that for $T \approx 10$ yr. Dee et al. (2017), however, discounted a SN as the cause of the stepwise increase because tree-ring records from other localities fail to show what should have been a global phenomenon.

Both Damon et al. (1995a, 1995b) and Miyake at al. (2012) considered SPEs arising from clusters of giant solar flares as an alternative explanation for stepwise increases in $\Delta^{14}C$. However, Damon et al. (1995a, 1995b) concluded that $\Delta^{14}C$ signatures of clusters of flares of the required energy are absent in the Seattle dataset between AD 1500 and 1954 (Stuiver and Braziunas 1993), and that such SPEs would therefore be unlikely at earlier times.

Additional stepwise increases in $\Delta^{14}C$, all $\leq$ 5‰, may be present in the Tucson dataset (supplementary Figure S1 and Table S2) at AD 1063, 1167, 1297, 1429, and 1448–1450. Possible stepwise decreases are less common, at AD 1182 and 1367, both about 5‰. All of these changes are comparable in amplitude to the Schwabe-like cycles, and therefore difficult to distinguish reliably.

Usoskin and Kovaltsov (2012) suggested large SPEs dated approximately at AD 1460 and 1505 on the basis of ^{10}Be data from an ice core at the South Pole. The stepwise change at AD 1448–1450 in the Tucson $\Delta^{14}C$ record (Figure 8) is 4.9‰, calculated as the difference between means for the preceding and following time intervals indicated by horizontal bars. The change coexists with a 5-yr decrease of about 0.6‰ in $\delta^{13}C$, which may indicate a climate effect corresponding to the change in $\Delta^{14}C$. We suggest that these stepwise changes correspond to the AD 1460 SPE, with better time resolution. A 5‰ stepwise change also appears to be present near AD 1450 in the $\Delta^{14}C$ record of Miyahara et al. (2006). At AD 1506–1507 in the Tucson dataset (Figure S1),

https://doi.org/10.1017/RDC.2019.27 Published online by Cambridge University Press

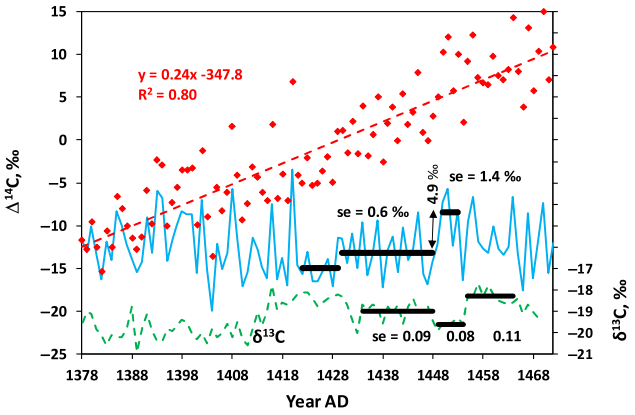

Figure 8 Tucson $\Delta^{14}C$ data, AD 1378–1472 (continuous curve), detrended using the linear regression shown (diamond symbols), compared with the Tucson $\delta^{13}C$ time series. Solid bars indicate mean $\Delta^{14}C$ and $\delta^{13}C$ (over the intervals indicated by bar length, with standard errors, se, indicated) around the 4.9‰ change in $\Delta^{14}C$ at AD 1450.

a series of declining $\Delta^{14}C$ values is abruptly interrupted by a 6‰ increase that is difficult to distinguish in form from neighboring Schwabe-like cycles (Figure S1).

A very large volcanic eruption that occurred in AD 1258 or 1259 (Emile-Geay et al. 2008) is not convincingly recorded in the Tucson $\Delta^{14}C$ and $\delta^{13}C$ records (supplementary Figure S1), but corresponds to a decade, beginning in AD 1256, of thin tree rings (supplementary Table S2).

THE $\delta^{13}C$ RECORD

The time-series of $\delta^{13}C$ and $\Delta^{14}C$ are broadly similar in form (Figures 1A ,1C, 9A). The $\delta^{13}C$ and $\Delta^{14}C$ time series, expressed as decadal averages in order to eliminate short-period noise, are most closely related in the interval AD 1100–1510, within which $R^2 = 0.69$ (Figure 9B). For the entire dataset, AD 998–1510, $R^2 = 0.53$, reflecting poor correlation in the interval AD 998–1100. The R^2 values have been calculated for decadal averages, beginning AD 1105, 1115 etc. (see Table S1); note that the values of R^2 are lower when calculated for decades beginning AD 1100, 1110, etc., e.g. 0.63 for AD 1100–1510. For both sets of decadal means, R^2 is maximized if $\delta^{13}C$ lags behind $\Delta^{14}C$ by 10 to 30 yr, or 130 to 140 yr (Figure 9C). This lag appears to be related to cycles with T near 110 yr in both datasets, causing R^2 to have a second maximum where the cycles realign with increasing applied lag. Lag between $\delta^{13}C$ and $\Delta^{14}C$ at millennial time scale is more difficult to determine in a dataset spanning 513 yr; using 100-yr means calculated every 25 yr (in order to remove short-period variations) suggests that R^2 is maximized if $\delta^{13}C$ lags behind $\Delta^{14}C$ by 25–50 yr (Figure 9C).

The changes in $\delta^{13}C$ reflect surface environmental factors, not the cosmogenic processes ultimately responsible for the $\Delta^{14}C$ time series. Carbon isotope discrimination between a C_3 plant (p) and air (a) is

$$\Delta_3 = \frac{\delta(a) - \delta(p)}{1 + 0.001\delta(p)} \approx \delta(a) - \delta(p) \quad (1)$$

https://doi.org/10.1017/RDC.2019.27 Published online by Cambridge University Press

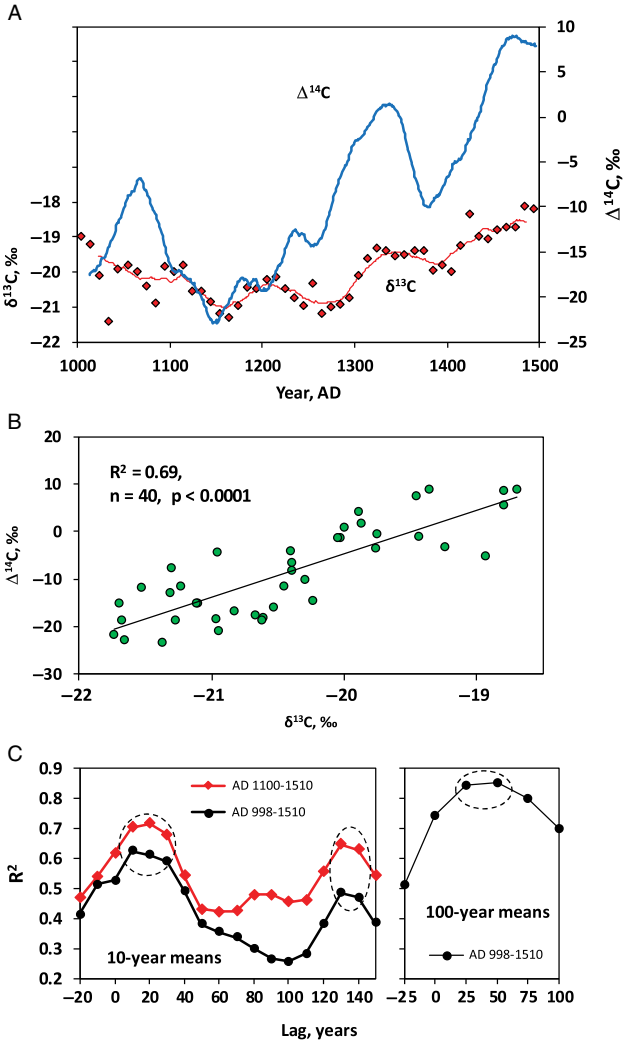

Figure 9 A. Time-series plot of decadal averages of $\Delta^{14}C$ and $\delta^{13}C$ for the Tucson dataset. B. $\Delta^{14}C$ vs. $\delta^{13}C$, for AD 1100–1510; the points represent decadal averages, beginning AD 1105, 1115 etc. (see Table S3); the value of R^2 is lower for decades beginning AD 1100, 1110, etc. C. Effect of time lag on correlation (R^2) of $\Delta^{14}C$ vs. $\delta^{13}C$ for decadal means, with separate calculations for AD 1100–1510 and AD 998–1510 (left), and for 100-yr means, calculated every 25 yr for AD 998–1510 (right). A positive lag signifies $\delta^{13}C$ lagging behind $\Delta^{14}C$. R^2 values within dashed ellipses have p values < 0.0001.

(Farquhar and Richards 1984) where the δ symbols (simplified to δ_p and δ_a below) denote $\delta^{13}C$. Values of δ_a have remained close to constant in the global atmosphere over the time interval AD 1000–1500, on the evidence of measurements in ice cores (e.g. Rubino et al. 2013). Persistent local inhomogeneities of 1‰ or more in δ_a are unlikely at annual to decadal time scales and have not been observed in recent decades (Carbon Dioxide Information Analysis Center 2010). Values of δ_p are therefore inversely related to values of Δ_3.

https://doi.org/10.1017/RDC.2019.27 Published online by Cambridge University Press

Relevant environmental variables at the study site include temperature, water availability (encompassing both relative humidity of air and availability of soil water) and irradiance (Farquhar et al. 1989; McCarroll and Loader 2004; Cernusak et al. 2013). Observed δ_p values result from the complex interplay of two biological functions: stomatal conductance, mediated by water availability, and photosynthetic rate, controlled by temperature and irradiance. Where plants are not subjected to extremes of stress from heat and dryness (as in the present study area), it is not possible to determine a simple causality for variations in δ_p (McCarroll and Loader 2004, and references therein). Nonetheless, three of the four variables are climatic in origin; the origin of the fourth, irradiance, is discussed below. Even though a positive correlation between Δ_3 and ambient temperature has been suggested from studies of lowland plants from various latitudes (Körner et al. 1991), and in individual plants (e.g., Leavitt and Long 1982), contrary results exist (McCarroll and Loader 2004). Likewise, although a global positive correlation has been suggested between Δ_3 and mean annual precipitation (Diefendorf et al. 2010) and in individual trees (e.g. Leavitt and Long 1991), studies reviewed by McCarroll and Loader (2004) indicate a complex dependence.

Irradiance correlates negatively with Δ_3 (Ehleringer et al. 1986; Leavitt and Long 1991). Ehleringer et al. (1986) observed decreases of about 4‰ in δ_p where irradiance was reduced by a factor of 2.3 because of shading. Annual solar irradiance changes by 6% owing to the elliptical geometry of the Earth's orbit (Floyd et al. 2002), and by a factor of 2 (neglecting absorption in the atmosphere) at 37°N as a result of seasonal change in the incident angle of solar radiation. The Schwabe cycle produces changes in solar irradiance in the visible spectrum that are much smaller, 0.1–0.38%, (Hoyt and Schatten 1997, p. 196 ff.). Change in visible irradiance between the Maunder Minimum and the present is likely to be of similar magnitude (Lean 2000). Photosynthetic effects of solar luminosity cycles are therefore small relative to those arising from shorter-term phenomena, and are unlikely to cause large changes in δ_p.

The effect of irradiance (governed by the amount of shading from tree canopies), combined with the effects of tree height on the availability of water in leaf tissue (governed by hydraulic conductivity in tree trunks) causes Δ_3 to decrease with tree height (Leavitt 2010; McDowell et al. 2011). Ambrose et al. (2009) measured the effect in leaves of contemporaneous individuals of *Sequoiadendron giganteum*, finding that Δ_3 decreased by 3–4‰ as tree height increased from 30 to 90 m, which can be compared with our observed increase of 3 to 3.5‰ in $\delta^{13}C$ of cellulose between AD 1150 and 1490 (Figure 1B). Most height-growth in sequoias takes place in the first 400 yr, but trunk volume continues to increase steadily until an age of at least 2500 yr in the case of the General Sherman tree (Weatherspoon 1990). Craig (1954) recorded an increase of 2‰ in $\delta^{13}C$ during the first 200 yr of growth of a sequoia, and little change in the succeeding 600 yr. The age of the tree sampled for this study was not noted by the samplers. However, the sampling of broader rings since AD 1024 probably represents the later phase of growth, with modest increase in height and thus little change in $\delta^{13}C$ attributable to tree growth.

Two possible explanations of the long-term changes in our $\delta^{13}C$ time series arise: (1) that the long-term increase in $\delta^{13}C$ is a consequence of growth of the tree, with secondary cyclic variations resulting from changes in environmental factors; and (2) that changes in $\delta^{13}C$ arise from the factors controlling $\Delta^{14}C$, i.e. that solar luminosity was modulating climate at the Big Stump Grove in such a way as to generate long-term trends in $\delta^{13}C$. If (1) is correct, then the long-term parallel changes in $\delta^{13}C$ and $\Delta^{14}C$ in the Tucson dataset

https://doi.org/10.1017/RDC.2019.27 Published online by Cambridge University Press

(Figures 1B, 9A) are coincidental. Our dataset shows a general decrease in $\delta^{13}C$ between AD 998 and AD 1150, inconsistent with the $\delta^{13}C$ change expected in early growth of a tree. This and the shared variance of $\delta^{13}C$ and $\Delta^{14}C$ favor explanation (2), notwithstanding our inability to identify causality in detail.

A complex interplay of environmental variables seems likely to be related to the noise in the annual $\delta^{13}C$ record (Figure 1C), and also to the lack of correspondence between the sequoia $\delta^{13}C$ record and dendrochronological records from the immediate region (Hughes and Brown 1992; Graumlich 1993; Scuderi 1993; Figure S2). Our sequoia $\delta^{13}C$ time series also bears no relationship (Figure 1B) to $\delta^{13}C$ in tree rings for multiple species at other locations over the same time interval (Stuiver and Braziunas 1987). The latter data are expressed as residuals of $\delta^{13}C$ (the differences between decadal $\delta^{13}C$ measurements and the pre-1850 mean $\delta^{13}C$ for each species) and have a range of 1.2‰, smaller than $\delta^{13}C$ ranges found in the Tucson dataset, namely 3.3‰ in decadal averages and 5.2‰ in annual measurements (Table S2, excluding a single outlier).

DISCUSSION: IMPLICATIONS FOR CLIMATE CHANGE

The $\delta^{13}C$ time series does not meet usual dendrochronological standards in that it is derived from a single tree. It is noisy, no doubt owing to short-term changes in environmental parameters (see previous section). Nonetheless, the time-series of $\Delta^{14}C$ and $\delta^{13}C$ in this study are strikingly similar in form with and without low-pass filtering (Figures 1 and 9A). The $\delta^{13}C$ signal—a change of 3.5‰ in the smoothed $\delta^{13}C$ time series—is large in the context of tree-ring isotope data (e.g. Körner et al. 1991; Leavitt and Long 1991; Leavitt 2010).

The $\Delta^{14}C$ time series provides a record originating as changes in cosmogenic production rates of ^{14}C and is attenuated and phase-shifted as described above (Background). The $\delta^{13}C$ time series provides a record of long-term change in multiple interacting environmental parameters. The long-term $\delta^{13}C$ record is therefore probably best explained as a product of climate change, the details of which cannot be deduced from $\delta^{13}C$ alone. The principal mode of variation of the $\Delta^{14}C$ and $\delta^{13}C$ time series in this study is part of a cycle with a period (T) of 850 to 1000 yr (Figure 2). A secondary cyclicity with T near 100 yr is also visible in both series.

A recent version of the dependence of ^{14}C phase shift on T (Beer et al. 2012, Figure 13.5.3.2-2) gives lags of 100–125 yr for $T = 1000$ yr between extrema of production of ^{14}C in the upper atmosphere (inversely related to extrema of solar luminosity) and subsequent, corresponding extrema archived at Earth's surface. For $T = 100$ yr, the lag is 10 yr. Earlier versions (Damon and Peristykh 2004; Usoskin and Kromer 2005) gave lags of 60–110 and 19–21 yr, respectively. The smoothed $\delta^{13}C$ time series expressed as 10-yr means (Figure 9A), lags behind the $\Delta^{14}C$ time series by 10 to 30 yr (Figure 9C). As explained above, this additional lag applies to the centennial cyclicity. For the millennial cycle of $\delta^{13}C$, an additional lag of 25–50 yr is suggested (Figure 9C). The Tucson dataset therefore indicates a lag (incorporating the phase-shift estimate of Beer et al. 2012) of 20–40 yr between extrema of the centennial cycles of solar luminosity and $\delta^{13}C$, an effect seen most clearly between AD 1100 and 1500. Less clearly, there appears to be a lag of 125–175 yr between extrema of the millennial cycles of solar luminosity and $\delta^{13}C$.

Helama et al. (2010), in a study comparing widths of tree rings from Arctic Scandinavia and reconstructed sunspot numbers over the past 2000 yr, concluded that the millennial component

https://doi.org/10.1017/RDC.2019.27 Published online by Cambridge University Press

of their tree-ring data lagged behind that of reconstructed sunspot numbers by 70–100 yr for the Late Holocene. If the long-term $\delta^{13}C$ signal in our dataset is indeed of climatic origin, then a similar, but larger, lag of climate behind solar luminosity is implied, regardless of whether we can identify the specific cause of the long-term change in $\delta^{13}C$. A similar lag of 20–40 yr for the centennial component is implied. The studies describe regional effects, in widely separated regions of contrasting climate. Both studies assume that the phase shifts calculated from models of the carbon cycle are correct.

The most recent grand solar maximum occurred between AD 1960 and 1980, according to sunspot numbers (e.g. SILSO, 2019). It is not yet clear whether this maximum represents the culmination of the millennial cycle or a maximum of the centennial cyclicity superimposed on the millennial cycle, in which case the post-1980 decrease in sunspot numbers would be analogous to the punctuation of the long Medieval Solar Maximum by the Oort minimum (Figure 2). Steinhilber and Beer (2013) deduced that the millennial grand maximum had occurred late in the 20th century, whereas Damon and Peristykh (2005) forecast it for about AD 2040. If the AD 1960–1980 grand maximum is of millennial time-scale, the corresponding peak climatic response, which may be more complex than warming alone, is predicted to lag behind the sunspot and luminosity maxima by at least a century, therefore occurring in the second half of the 21st century. This study suggests that peak climatic response to a centennial AD 1960–1980 grand maximum would end before AD 2020, but that the response to the underlying millennial component of increasing solar luminosity would continue into and possibly beyond the second half of the 21st century.

Predicting the magnitude of such climate response in relation to that arising from greenhouse gases is not straightforward. Two contrasting opinions are present in the literature. According to the first, the influence of solar activity is miniscule in comparison to the effect of anthropogenic greenhouse gases. Myhre et al. (2013) and Masson-Delmotte et al. (2013) in their reviews for the Intergovernmental Panel on Climate Change (IPCC) concluded that the radiative forcing attributable to changes in total solar irradiance (TSI) is small during Schwabe cycles, less than 1% of the radiative forcing due to greenhouse gases. That claim appears to be based on satellite measurements of TSI, modeled estimates of anthropogenic effects, and temperature observations during recent solar cycles. The authors suggested further that the amplitude of cyclic variations in TSI due to the Schwabe cycle is approximately the same as that due to the transition from the Maunder minimum to the modern grand solar maximum. The magnitude of the latter is less certain than that of the former.

According to the second opinion, the component of climate change due to solar radiative forcing is larger than that corresponding to the IPCC opinion. Direct observation and climate proxy archives show clear evidence of changes due to solar luminosity cycles at the time scale of the Schwabe cycle (e.g. Rigozo et al. 2007; Meehl et al. 2009; Perone et al. 2016) and at longer time scales (e.g. Mann et al. 1998; Yu and Ito 1999; Eichler et al. 2009; Beer et al. 2012, Figure 17.5–2; Soon et al. 2015). Damon and Peristykh (2005) estimated that 18% of 20th-century global warming was attributable to solar forcing. Possible mechanisms may involve (1) heating of the troposphere and upper stratosphere as a result of the formation and destruction of ozone by incident ultraviolet radiation (Hoyt and Schatten 1997; Meijer et al. 1999; Floyd et al. 2002) and (2) enhancement of cloud formation in the stratosphere when cosmic ray flux is high (Meijer et al. 1999; Solanki and Krivova 2003). In the far and middle ultraviolet spectral regions, relative cyclic variations

https://doi.org/10.1017/RDC.2019.27 Published online by Cambridge University Press

are larger in amplitude than for TSI, and are as much 20–100% in the far ultraviolet spectral region responsible for tropospheric ozone formation (e.g. Lean et al. 1995; Lean 2000; Bolduc et al. 2014). Mechanism (1) is not yet understood in terms of its downward propagation to Earth's surface. If the mechanism involves the downward transfer of heat, oxygen ions or ozone molecules (Floyd et al. 2002), then amplitude modification and phase shift dependent on the periodicity of solar luminosity are likely as each component is distributed among "boxes." Such processes would be analogous to those modeled for ^{14}C in the carbon-cycle box models. Phase shifts are therefore plausible for mechanism (1), but less so for mechanism (2), which involves direct insolation at Earth's surface. Meehl et al. (2009) observed enhanced precipitation, decreased sea surface temperatures and reduced low-latitude clouds in the tropical Pacific Ocean during maximum years of the Schwabe cycle, observations of a scale requiring an amplification of the Schwabe cycle in the atmosphere. The IPCC opinion on solar radiative forcing is no doubt correct in attributing the largest component of 20th-century climatic warming to the greenhouse effect. However, the component due to solar radiative forcing may be larger than that indicated by changes in TSI.

If the prediction of a delay in the effects of the most recent grand solar maximum is correct, a non-negligible climate response from that source may be occurring at present, or may yet occur. We observe that solar luminosity cycles of longer period differ from Schwabe cycles in providing sustained high solar irradiance over decades (the Modern Grand Solar Maximum) to a century or more (the Early and Late Medieval Solar Maxima). The climatic effects of solar variation at millennial and centennial scales may therefore be greater than those of Schwabe cycles.

CONCLUSIONS

Time series (Tucson dataset) of $\Delta^{14}C$ and $\delta^{13}C$ with annual resolution, representing the years AD 998–1510, have been measured in tree rings of a single sequoia from the Big Stump Grove, California. The Tucson data, together with data for other field locations from laboratories in Seattle and Nagoya, provide a high-resolution record of $\Delta^{14}C$ for AD 600–1954.

The Tucson sequoia data, reduced to decadal means, compare closely with decadal data for AD 1000–1510 measured on Douglas fir by the Seattle laboratory. Differences between the decadal data are non-random, changing in sign with time.

Discrete Fourier Transform analysis reveals short-term periods of 126, 56, 17.6, 13.6, 10.4, and 7.1 yr, similar to those of the Seattle data for AD 1500–1954. The 56-yr period persists from AD 1000–1200 and AD 1350–1400, but is weak or absent at other times. Short-term cycles resembling Schwabe cycles, with periods of 10–17 yr, appear to be observed between AD 1000 and 1120, and have amplitudes of 3–6‰; however, analytical uncertainty renders such observations problematic. Short term cycles with periods near 7 yr are prominent between AD 1320 and 1450 and have amplitudes as high as 10‰.

Possible stepwise increases in $\Delta^{14}C$ are mainly 5‰ or less, and therefore difficult to distinguish from Schwabe and other short-period cycles. A stepwise increase at AD 1450 may correspond to a large solar proton event recognized at about AD 1460 in ^{10}Be data.

Smoothed time series of $\Delta^{14}C$ and $\delta^{13}C$ show similar forms and correlate most closely if $\delta^{13}C$ lags behind $\Delta^{14}C$ by 10–30 yr (centennial-scale cyclicity) and possibly 25–50 yr (millennial-scale). The $\delta^{13}C$ time series may represent a regional climate signal related to solar

https://doi.org/10.1017/RDC.2019.27 Published online by Cambridge University Press

luminosity, but lagging behind it by 125–175 yr for the millennial cycle, and 20–40 yr for centennial cycles. Peak climate response resulting from the modern grand solar maximum may occur with a delay of decades to over a century, and may be larger in relation to greenhouse-induced warming than has been predicted by the IPCC.

ACKNOWLEDGMENTS

The authors acknowledge the role of the late Professor Paul Damon in initiating and completing much of the research reported here, and of the late Professor Austin Long, in whose laboratory the measurements were undertaken. Alexei Peristykh carried out the spectral analysis of the ^{14}C time series. The authors express their gratitude to Dr. Paula Reimer and to two anonymous reviewers whose comments greatly improved the manuscript. The research was funded by several grants from the National Science Foundation, viz. ATM 0226063, ATM-0210091, ATM-024710, ATM-9520135, ATM-8919535 EAR-8822292 and by the State of Arizona.

SUPPLEMENTARY MATERIAL

To view supplementary material for this article, please visit https://doi.org/10.1017/RDC.2019.27

REFERENCES

Ambrose AR, Sillett SC, Dawson TE. 2009. Effects of tree height on branch hydraulics, leaf structure and gas exchange in California redwoods. Plant Cell Environment 32(7):743–757.

Bard E, Raisbeck G, Yiou F, Jouzel J. 1997. Solar modulation of cosmogenic nuclide production over the last millennium: comparison between ^{14}C and ^{10}Be records. Earth and Planetary Science Letters 150(3–4):453–462.

Beer J, McCracken K, von Steiger R. 2012. Cosmogenic radionuclides: theory and applications in the terrestrial and space environments. Berlin (Germany): Springer. doi: 10.1007/978-3-642-14651-0.

Bolduc C, Charbonneau P, Barnabé R, Bourqui MS. 2014. A reconstruction of ultraviolet spectral irradiance during the Maunder Minimum. Solar Physics 289(8):2891–2906. doi: 10.1007/s11207-014-0503-0.

Carbon Dioxide Information Analysis Center Monthly Atmospheric $^{13}C/^{12}C$ Isotopic Ratios for 11 SIO Stations. 2010. Berkeley (CA): United States Department of Energy; [accessed 2019 Jan 28]. http://cdiac.ess-dive.lbl.gov/trends/co2/iso-sio/iso-sio.html.

Cernusak LA, Ubierna N, Winter K, Holtum JAM, Marshall JD, Farquhar GD. 2013. Environmental and physiological determinants of carbon isotope discrimination in terrestrial plants. New Phytologist 200:950–965.

Craig H. 1954. Carbon-13 variations in sequoia rings and the atmosphere. Science 119(3083): 141–143.

Damon PE, Eastoe CJ, Hughes MK, Kalin RM, Long A, Peristykh AN. 1998. Secular variation of $\Delta^{14}C$ during the Medieval Solar Maximum: a progress report. In: Mook WG, van der Plicht J, editors. Proceedings of the 16th International ^{14}C Conference. Radiocarbon. 40(1):343–350.

Damon PE, Dai K, Kocharov GE, Mikheeva IB, Peristykh AN. 1995a. Radiocarbon production by the gamma-ray component of supernova explosions. In: Cook GT, Harkness DD, Miller BF, Scott EM, editors. Proceedings of the 15th International ^{14}C Conference. Radiocarbon 37(2):599–604.

Damon PE, Kocharov GE, Peristykh AN, Mikheeva IB, Dai K. 1995b. High energy gamma rays from SN1006 AD. Proceedings of the International Cosmic Ray Conference, Rome 2:311–314.

Damon P, Eastoe CJ, Mikheeva IB. 1999. The Maunder Minimum: an interlaboratory comparison of $\Delta^{14}C$ from AD 1688 to AD 1710. Radiocarbon 41(1):47–50.

Damon PE, Peristykh AN. 2000. Radiocarbon calibration and application to geophysics, solar physics, and astrophysics. Radiocarbon 42(1): 137–150.

Damon PE, Peristykh AN. 2004. Solar and climatic implications of the centennial and millennial periodicities in atmospheric $\Delta^{14}C$ variations. American Geophysical Union Geophysical Monograph 141:237–249.

Damon PE, Peristykh AN. 2005. Solar forcing of global temperature change since AD 1400. Climate Change 68(1):101–111.

Damon PE, Sonnett CP. 1991. Solar and terrestrial components of the atmospheric ^{14}C variation spectrum. In: Sonnett CP, Giampapa MS, Matthews MS. editors. The Sun in time. Tucson (AZ): Univ. of Ariz. Press. p. 366–388.

Dee M, Pope B, Miles D, Manning S, Miyake F. 2017. Supernovae and single-year anomalies in the atmospheric radiocarbon record. Radiocarbon 59(2):293–302. doi: 10.1017/RDC.2016.50.

Diefendorf AF, Mueller KE, Wing SL, Koch PL, Freeman KH. 2010. Global patterns in leaf ^{13}C discrimination and implications for studies of past and future climate. PNAS 107(13): 5738–5743.

Ehleringer JR, Field CB, Lin ZF, Kuo CY. 1986. Leaf carbon isotope and mineral composition in subtropical plants along an irradiance cline. Oecologia 70(4):520–526.

Eichler A, Olivier S, Henderson K, Laube A, Beer J, Papina T, Gäggeler HW, Schwikowski M. 2009. Temperature response in the Altai region lags solar forcing. Geophysical Research Letters 36(1): L01808. doi: 10.1029/2008GL035930.

Emile-Geay J, Seager R, Cane M, Cook E, Haug GH. 2008. Volcanoes and ENSO over the past millennium. Journal of Climate 21(13): 3134–3148.

Farquhar GD, Ehleringer JR, Hubick KT. 1989. Carbon isotope discrimination and photosynthesis. Annual Review of Plant Physiology and Plant Molecular Biology 40(1): 503–537.

Farquhar GD, Richards RA. 1984. Isotopic composition of plant carbon correlates with water-use efficiency in wheat genotypes. Australian Journal of Plant Physiology 11(6): 539–552.

Floyd LE, Tobiska WK, Cebula RP. 2002. Solar UV irradiance, its variation, and its relevance to the Earth. Advances in Space Research 29(10):1427–1440.

Graumlich LJ. 1993. A 1000-year record of temperature and precipitation in the Sierra Nevada. Quaternary Research 39(2):249–255.

Güttler D, Wacker L, Kromer B, Friedrich M, Synal H-A. 2013. Evidence of 11-year solar cycles in tree rings from 1010 to 1110 AD—Progress on high precision AMS measurements. Nuclear Instruments and Methods in Physics Research B 294:459–463

Helama S, Fauria M, Mielikainen K, Timonen M, Eronen M. 2010. Sub-Milankovitch solar forcing of past climates: mid and late Holocene perspectives. Geological Society of America Bulletin 122(11/12):1981–1988.

Houtermans JC, Suess HS, Oeschger H. 1973. Reservoir models and production rate variations of natural radiocarbon. Journal of Geophysical Research 78(12):1897–1908.

Hoyt DV, Schatten KH. 1997. The role of the Sun in climate change. Oxford (UK): Oxford University Press. 279 p.

Hughes MK, and Brown PM. 1992. Drought frequency in central California since 101 B.C. recorded in giant sequoia tree rings. Climate Dynamics 6(3–4):161–167.

Hughes MK, Touchan R, Brown PM. 1996. A multimillennial network of giant sequoia chronologies for dendroclimatology. In: Dean JS, Meko DM, Swetnam TW, editors. Tree rings, environment and humanity. Tucson (AZ): Radiocarbon. p. 225–234.

Jull AJT, Panyushkina IP, Lange TE, Kukarskih VV, Myglan VS, Clark KJ, Salzer MW, Burr GS, Leavitt SW. 2014. Excursions in the ^{14}C record at A.D. 774–775 in tree rings from Russia and America. Geophysical Research Letters 41(8): 3004–3010. doi: 10.1002/2014GL059874.

Kalin RM, McCormac FG, Damon PE, Eastoe CJ, Long A. 1995. Intercomparison of high–precision ^{14}C measurements at the University of Arizona Radiocarbon Laboratory. Radiocarbon 37(1):33–38.

Kocharov GE. 1992. Radiocarbon and astrophysical-geophysical phenomena. In: Taylor RE, Long A, Kra RS, editors. Radiocarbon after four decades. New York (NY): Springer-Verlag. p. 130–145.

Körner C, Farquhar GD, Wong SC. 1991. Carbon isotope discrimination by plants follows latitudinal and altitudinal trends. Oecologia 88(1):30–40.

Lean J. 2000. Evolution of the Sun's spectral irradiance since the Maunder Minimum. Geophysical Research Letters 27(16):2425–2428.

Lean JL, Hulburt EO, White OR, Skumanich A. 1995. On the solar ultraviolet spectral irradiance during the Maunder Minimum. Global Biogeochemical Cycles 9(2):171–182.

Leavitt SW. 2010. Tree-ring C-H-O isotope variability and sampling. Science of the Total Environment 408(22):5244–5253.

Leavitt SW, Long A. 1982. Evidence for $^{13}C/^{12}C$ fractionation between tree leaves and wood. Nature 298(5876):742–744.

Leavitt SW, Long A. 1991. Seasonal stable-carbon isotope variability in tree rings: possible paleoenvironmental signals. Chemical Geology (Isotope Geoscience Section) 87(1):59–70.

Mann ME, Bradley RS, Hughes ML. 1998. Global-scale temperature patterns and climate forcing over the past six centuries. Nature 392(6678): 779–787.

Masson-Delmotte V, Schulz M, Abe-Ouchi A, Beer J, Ganopolski A, González Rouco JF, Jansen E, Lambeck K, Luterbacher J, Naish T, et al. 2013. Information from paleoclimate archives. In: Stocker TF, Qin D, Plattner G-K, Tignor M, Allen SK, Boschung J, Nauels A, Xia Y,

Bex V, and Midgley PM, editors. Climate Change 2013: the physical science basis. contribution of Working Group I to the Fifth Assessment Report of the Intergovernmental Panel on Climate Change. Cambridge (UK): Cambridge University Press. p. 383–464.

McCarroll D, Loader NJ. 2004. Stable isotopes in tree rings. Quaternary Science Reviews 23(7–8): 771–801.

McCormac F, Baillie M, Pilcher J, Kalin R. 1995. Location-dependent differences in the ^{14}C content of wood. Radiocarbon 37(2):395–407.

McCormac FG, Hogg AG, Higham TFG, Lynch-Stieglitz J, Broecker WS, Baillie MGL, Palmer J, Xiong L, Pilcher JR, Brown D,, et al. 1998. Temporal variation in the interhemispheric C-14 offset. Geophysical Research Letters 25(9):1321–1324.

McDowell NG, Bond BJ, Dickman LT, Ryan MG, Whitehead D. 2011. Relationships between tree height and carbon isotope discrimination. In: Meinzer FC, Lachenbruch B, Dawson TE, editors. Size- and age-related changes in tree structure and function. New York (NY): Springer. p. 255–285.

Meehl GA, Arblaster JM, Matthes K, Sassi F, van Loon H. 2009. Amplifying the Pacific climate system response to a small 11-year solar cycle forcing. Science 325(5944):1114–1118.

Meijer HAJ, Dergachev VA, van der Plicht J, Renssen H, Raspopov OM, van Geel B. 1999. The role of solar forcing upon climate change. Quaternary Science Reviews 18(3):331–338.

Miyahara H, Masuda K, Muraki Y, Kitagawa H, Nakamura T. 2006. Variation of solar cyclicity during the Spoerer Minimum. Journal of Geophysical Research 111:A03103. doi: 10.1029/2005JA011016.

Miyahara H, Masuda K, Nagaya K, Kuwana K, Muraki H, Nakamura T. 2007. Variation of solar activity from the Spoerer to the Maunder minima indicated by radiocarbon content in tree rings. Advances in Space Research 40(7):1060–1063. doi: 10.1016/j.asr.2006.12.04.

Miyahara H, Masuda K, Furuzawa H, Menjo H, Muraki Y, Kitagawa H, Nakamura T. 2004. Variation of the radiocarbon content in tree rings during the Spoerer minimum. Radiocarbon 46(2):965–968.

Miyahara H, Yokoyama Y, Masuda K. 2008. Possible link between multi-decadal climate cycles and periodic reversals of solar magnetic field polarity. Earth and Planetary Science Letters 272(1–2):290–295. doi: 10.1016/j.epsl.2008.04.050.

Miyahara H, Yokoyama Y, Yamaguchi YT. 2009. Influence of the Schwabe/Hale solar cycles on climate change during the Maunder Minimum. In: Kosovichev AG, Andrei AH, Rozelot J-P, editors. Solar and stellar variability: impact on earth and planets. Proceedings IAU Symposium. 5(S264):427–433. doi: 10.1017/S1743921309993048

Miyake F, Nagaya K, Masuda K, Nakamura T. 2012. A signature of cosmic-ray increase in AD 774–775 from tree rings in Japan. Nature 486(7402):240–242. doi: 10.1038/nature11123.

Miyake F, Masuda K, Nakamura T. 2013a. Lengths of Schwabe cycles in the seventh and eighth centuries indicated by precise measurement of carbon-14 content in tree rings. Journal of Geophysical Research: Space Physics 118(12):7483–7487. doi: 10.1002/2012JA018320.

Miyake F, Masuda K, Nakamura T. 2013b. Another rapid event in the carbon-14 content of tree rings. Nature Communications 4:1748. doi: 10.1038/ncomms278.

Myhre G, Shindell D, Bréon F-M, Collins W, Fuglestvedt J, Huang J, Koch D, Lamarque J-F, Lee D, Mendoza B, et al. 2013. Anthropogenic and Natural Radiative Forcing. In: Stocker TF, Qin D, Plattner G-K, Tignor M, Allen SK, Boschung J, Nauels A, Xia Y, Bex V, Midgley PM, editors. Climate Change 2013: The physical science basis. Contribution of Working Group I to the Fifth Assessment Report of The Intergovernmental Panel on Climate Change. Cambridge (UK): Cambridge University Press. p. 659–740.

Oeschger H, Beer J. 1990. The past 5000 years history of solar modulation of cosmic radiation from ^{10}Be and ^{14}C studies Philosophical Transactions of the Royal Society of London. Series A, Mathematical and Physical Sciences 330(1615):471–480.

Pearson GW, Qua F. 1993. High-precision ^{14}C measurement of Irish oaks to show the natural ^{14}C variations from AD 1840–5000 BC: a correction. Radiocarbon 35(1):105–124.

Pearson GW, Pilcher JR, Baillie MGL, Corbett DM, Qua F. 1986. High-precision C-14 measurement of Irish oaks to show the natural C-14 variations from AD 1840 to 5210 BC. Radiocarbon 28(2B):911–934.

Perone A, Lombardi F, Marchetti M, Tognetti R, Lasserre B. 2016. Evidence of solar activity and El Niño signals in tree rings of Araucaria araucana and A. angustifolia in South America. Global and Planetary Change 145:1–10.

Raisbeck GM, Yiou F, Jouzel J, Petit JR. 1990. ^{10}Be and δ^2H in polar ice cores as a probe of the solar variability's influence on climate. Philosophical Transactions of the Royal Society of London. Series A, Mathematical and Physical Sciences 330(1615):463–470.

Reimer PJ, Baillie MGL, Bard E, Bayliss A, Beck JW, Bertrand CJH, Blackwell PG, Buck CE, Burr GS, Cutler KB, et al. 2004. IntCal04 terrestrial radiocarbon age calibration, 0–26 cal kyr BP. Radiocarbon 46(3):1029–1058.

Rigozo NR, Nordemann DJN, Evangelista da Silva H, de Souza Echer MP, Echer E. 2007. Solar and climate signal records in tree ring width

from Chile (AD 1587–1994). Planetary and Space Science 55(1):158–164.

Rubino M, Etheridge DM, Trudinger CM, Allison CE, Battle MO, Langenfelds RL, Steele LP, Curran M, Bender M, White JWC, et al. 2013. A revised 1000 year atmospheric $\delta^{13}C$-CO_2 record from Law Dome and South Pole, Antarctica. Journal of Geophysical Research: Atmospheres 118(15):8482–8499.

Scuderi LA. 1993. A 2000-year tree ring record of annual temperatures in the Sierra Nevada Mountains. Science 259(5100):1433–1436.

SILSO Sunspot index and long-term solar observation. 2019. Brussels [Belgium]: Royal Observatory of Belgium; [accessed 2019 Jan 28]. http://www.sidc.be/silso/yearlyssnplot.

Solanki SK, Krivova NA. 2003. Can solar variability explain global warming since 1970? Journal of Geophysical Research 108(A5):1200. doi: 10.1029/2002JA009753.

Soon W, Connolly R, Connolly M. 2015. Re-evaluating the role of solar variability on Northern Hemisphere temperature trends since the 19th century. Earth-Science Reviews 150: 409–452.

Steinhilber F, Beer J. 2013. Prediction of solar activity for the next 500 years. Journal of Geophysical Research: Space Physics 118(5):1861–1867. doi: 10.1002/jgra.50210.

Stuiver M, Polach HA. 1977. Discussion: reporting of ^{14}C data. Radiocarbon 19(3):355–363.

Stuiver M, Braziunas TF. 1987. Tree cellulose $^{13}C/^{12}C$ isotope ratios and climatic change. Nature 328(6125):58–60.

Stuiver M, Becker B. 1993. High-precision decadal calibration of the radiocarbon time scale, AD 1950–6000 BC. Radiocarbon 35(1):35–66.

Stuiver M, Braziunas TF. 1993. Sun, ocean, climate and atmospheric $^{14}CO_2$: an evaluation of causal and spectral relationships. The Holocene 3(4):289–305.

Stuiver M, Reimer PJ, Braziunas TF. 1998. High-precision radiocarbon age calibration for terrestrial and marine samples. Radiocarbon 40(3):1127–1151.

Swetnam TW, Baisan CH. 2003. Tree-ring reconstructions of fire and climate history in the Sierra Nevada and southwestern United States. In: Veblen TT, Baker WL, Montenegro G, Swetnam TW, editors. Fire and climatic change in temperate ecosystems of the western Americas. New York (NY): Springer-Verlag. p. 158–195.

Usoskin IG, Kovaltsov GA. 2012. Occurrence of extreme solar particle events: assessment from historical proxies. Astrophysical Journal 757(1):1–6. doi: 10.1088/0004-637X/757/1/92.

Usoskin IG, Kromer B. 2005. Reconstruction of the ^{14}C production rate from measured relative abundance. Radiocarbon 47(1):31–37.

Weatherspoon CP. 1990. Sequoiadendron giganteum (Lindl.) Buchholz Giant Sequoia. Taxodiaceae Redwood family. In: Bums RM, Honkala BH, technical coordinators. Silvics of North America, Volume 1. Conifers. Agriculture Handbook 654. Washington (DC): U.S. Department of Agriculture. p. 552–562.

Witkin DB. 1992. Production of impurities in benzene synthesis for liquid scintillation counting and its effect on high-precision radiocarbon measurements [thesis]. Tucson (AZ): University of Arizona.

Yu Z, Ito E. 1999. Possible solar forcing of century-scale drought frequency in the northern Great Plains. Geology 27(3):263–266.